NASA Contractor Report 168154

NASA-CR-168154
19830018985

CRACK LAYER MORPHOLOGY AND TOUGHNESS CHARACTERIZATION IN STEELS

Alexander Chudnovsky and Michael Bessendorf

Case Western Reserve University
Department of Civil Engineering
Cleveland, Ohio 44106

May 1983

Prepared for

NATIONAL AERONAUTICS AND SPACE ADMINISTRATION
Lewis Research Center
Under Grant NAG 3-223

TABLE OF CONTENTS

CHAPTER I

INTRODUCTION

There are two alternative approaches to the study of the laws of crack propagation and toughness characterization. The fracture mechanics approach is concerned with the stress intensity factor K or energy release rate J which are derived using the concepts of continuum mechanics. The material science approach concentrates on knowledge of the hierarchy of defects, their development, and interactions; that is, this approach emphasizes the micromechanisms of fracture processes. In the current work one of the possible ways of unifying these two approaches based on the CL theory is discussed.

The analysis of the critical energy release rate G_c shows that this parameter is history dependent. This is also supported by our findings. In addition, observations of the kinetics of crack growth show nonmonotonic crack advance under monotonic changes of energy release rate J (or stress intensity factor K). This implies the existence of intrinsic properties of the material which are not reflected by the G_c, K_c, J and K parameters. In many studies on the morphology of regions around the crack [1-6], the complex processes of the generation and development of microdefects on different hierarchial levels are observed. Perhaps parameters like K and yield stress σ_y are not sufficient to describe these fracture processes. For example, we observe entirely different shapes of the damage zones for different steels under similar loading conditions.

The recently proposed crack layer (CL) theory [7, 8 , 9] considers the crack together with the surrounding cloud of defects as one system which has several degrees of freedom. In the CL an active zone, where the nucleation and development of defects occur, can be distinguished. The

active zone (denoted in the literature as a process zone) and the wake zone are both distinct in the CL.

The motion of the active zone is decomposed into translation, rotation, and deformation. The generalized forces associated with the above mentioned degrees of freedom are derived within the framework of the thermodynamics of irreversible processes. These generalized forces are represented by linear functions of path-independent integrals J_1, L, M [10] and by integral characteristics of damage R_1, $R_{[kl]}$, R_o. Consequently the CL theory defines the relationship between the parameters of fracture mechanics and the characteristics of microstructural changes which are the subject of material science. Experimental study of the CL theory predictions and formulation of a suitable damage parameter are the ultimate goals of this work.

The toughness characteristic is represented as the product of the specific enthalpy of damage and integral cross section damage R_1. The former (enthalpy) is a candidate for being the material constant according to the CL theory. The latter (R_1) is history-dependent and is responsible for the widely observed changes of G_c.

Introduction of the R_1 parameter and its evolution are based on the analysis of the morphology of defects. The calculation of J or K is based on stress analysis and macroscopical measurements, for this reason complementary macro- and micro-experiments were carried out simultaneously. These experimental procedures are described in Chapter II. The results of the observations are presented in Chapter III. Chapter IV contains the analysis of the results, comparisons with the theoretical predictions, and interpretation of the data.

Dr. A. R. Rosenfield of Battelle-Columbus Laboratories made many helpful suggestions.

CHAPTER II

DESCRIPTION OF EXPERIMENTAL PROCEDURES

This study establishes the relationship of material toughness and the macroscopic process of crack growth with microscopic changes. The research described herein consists of both macro- and microscopic studies and the micro-macro relationship.

A. The macroscopic studies included inquiries into the characterization of material toughness and the kinetics of crack propagation.

1. Toughness Characterization Test

Samples with cracks of specified length, grown under sinusoidal tension-tension loading conditions, were subjected to the standard test for fracture toughness evaluation. This procedure uses three samples to obtain one data point. The AISI 302, 305 stainless , and 1070 carbon steels were used in this investigation. Data on fracture toughness parameters usually show large scatter [11]. In order to obtain statistically representative data, an ensemble of identical samples was prepared. The geometry of the samples is 150mm in length and 20mm in width. The thickness for each particular material was fixed. For different materials the thickness varied from 0.15mm to 0.5mm. A sixty degree notch was cut in the middle of a long side of each specimen. The ensemble included eight groups of 10 samples each. In each group of samples, cracks were grown to a specified length using sinusoidal tension-tension testing conditions ($R = \sigma_{min}/\sigma_{max} = 1/3$, average stress $\sigma_{av} = 150\ MNm^{-2}$, frequency $\nu = 50$ Hz, room temperature $T = 20^{o}C$). All the samples were then subjected to the standard test for fracture toughness evaluation. The maximum pulling force was recorded automatically. The critical crack length ℓ_c was measured on the fracture surface where the boundary between fatigue crack growth and unstable failure could be clearly identified.

2. Test for Kinetics of Crack Layer Propagation

The study of CL propagation was conducted on AISI 302 and 304 stainless steels and 1070 carbon steel. The geometry of the samples is the same as described above. A 20 KN capacity electrohydraulic closed loop MTS fatigue machine was used to conduct the constant amplitude, sinusoidal waveform, tension-tension cyclic loading. The samples were electrolytically polished prior to fatigue testing in Jacquet reagent [12] to reduce surface stresses and to obtain a mirrored surface for microscopic studies. The crack advance was registered on the attached scale using a travelling optical microscope. This microscope was attached to the MTS machine (see Figure 1) to control and register crack and surrounding damage evolution.

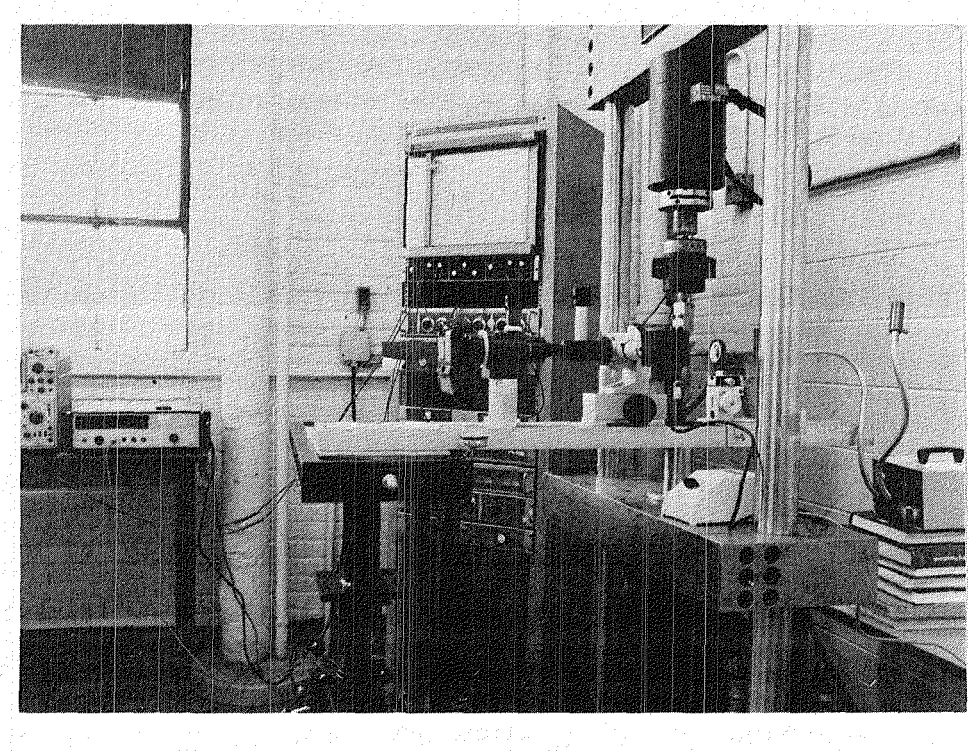

FIGURE 1

MTS fatigue machine with attached travelling optical microscope.

B. Microscopic studies consisted of direct observation of the CL propagation, analysis of dislocation density, and study of discontinuity surfaces. The damage zone surrounding the crack was observed through metallographic and SEM microscopes at magnifications of 50X, 100X, 250X, 500X, 1000X, 10,000X and 20,000X in order to identify quantitatively the primary elements of damage. A general picture of the CL was constructed from fragments of both side and top views.

A profile of dislocation density was obtained by a systematic mapping of the hardness measurements taken in the region of the crack tip [5, 13, 14] . Figure 2 shows the grid of the actual measurement points in the vicinity of the crack tip.

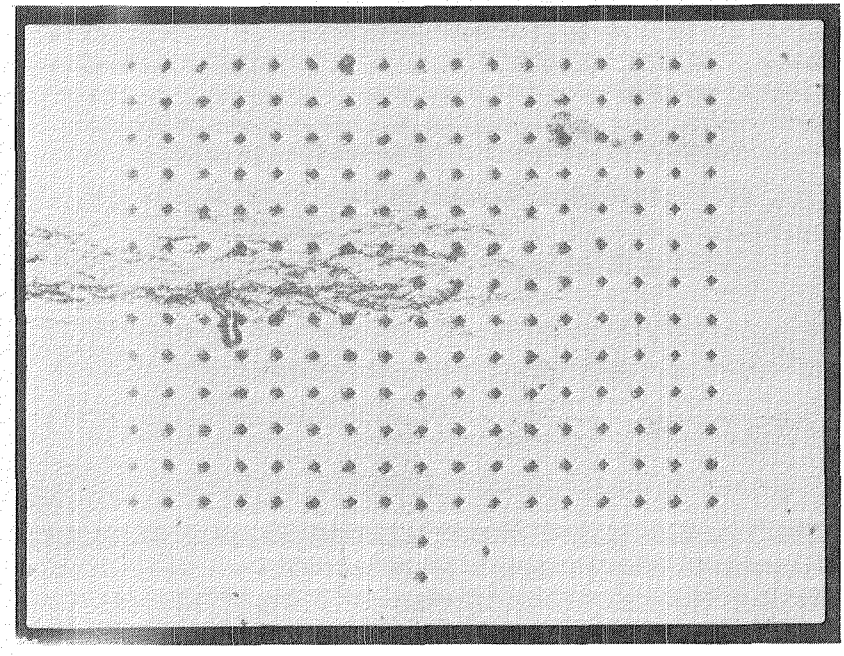

FIGURE 2

Picture of the actual grid consisting of microhardness dents on the surface of the fatigue crack specimen in the region of the crack tip. The spacing between the centers of the indents in x and y directions is 100 μm.

Discontinuities around the crack, which can be identified at 250X and higher magnifications were measured as follows. A grid consisting of two

orthogonal sets of parallel lines was superimposed on the picture taken at 500X magnification (Figure 3). Discontinuities had a prefered orientation. Therefore, the method of biased sampling was employed to obtain statistics of discontinuities [15]. The density of discontinuities is calculated on the basis of the number of intersections of the testing line with the traces of discontinuity surfaces [2,16,17].

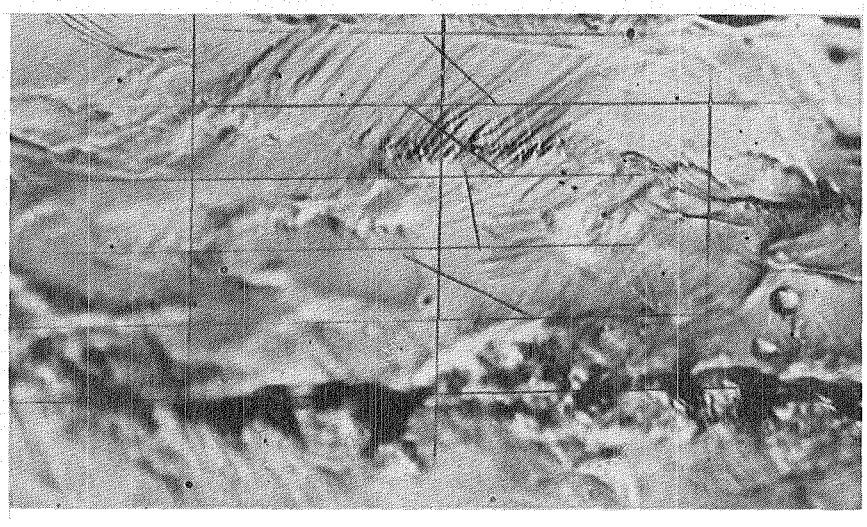

FIGURE 3

Grid for statistical analysis of discontinuous surfaces.

CHAPTER III

EXPERIMENTAL RESULTS

A. Phenomenological Study of Toughness Characterization

The goal of the current study is to examine the loading history-dependence of G_c. We consider the simplest loading history: the constant amplitude sinusoidal tension-tension loading. For these loading conditions the maximum local stresses in the vicinity of the growing crack tip monotonically increase with the crack length. Therefore, the J integral alone is sufficient to characterize the particular loading history. We use the value of J at the end of the fatigue stage 'J_h' as the parameter to reflect the history of loading. Figure 4 shows the dependence of the critical energy release rate G_c on J_h for three different materials. This dependence was obtained in accordance with experimental procedures outlined in the previous section. The points represented by symbols in Figure 4 are the results of three independent tests.

The critical energy release rate was calculated using the following expression:

$$G_c = \sigma_c^2 \pi \ell_c F^2(\ell_c/b) E^{-1} \qquad (1)$$

where σ_c is the failure stress, $F(\ell/b)$ is a geometrical factor calculated as,

$$F(\ell/b) = \sqrt{\frac{2b}{\ell} \operatorname{tg} \frac{\pi \ell}{2b}} \cdot \frac{0.752 + 2.02\ (\ell/b) + 0.37(1-\sin \frac{\pi \ell}{2b})^3}{\cos \frac{\pi \ell}{2b}} \qquad (2)$$

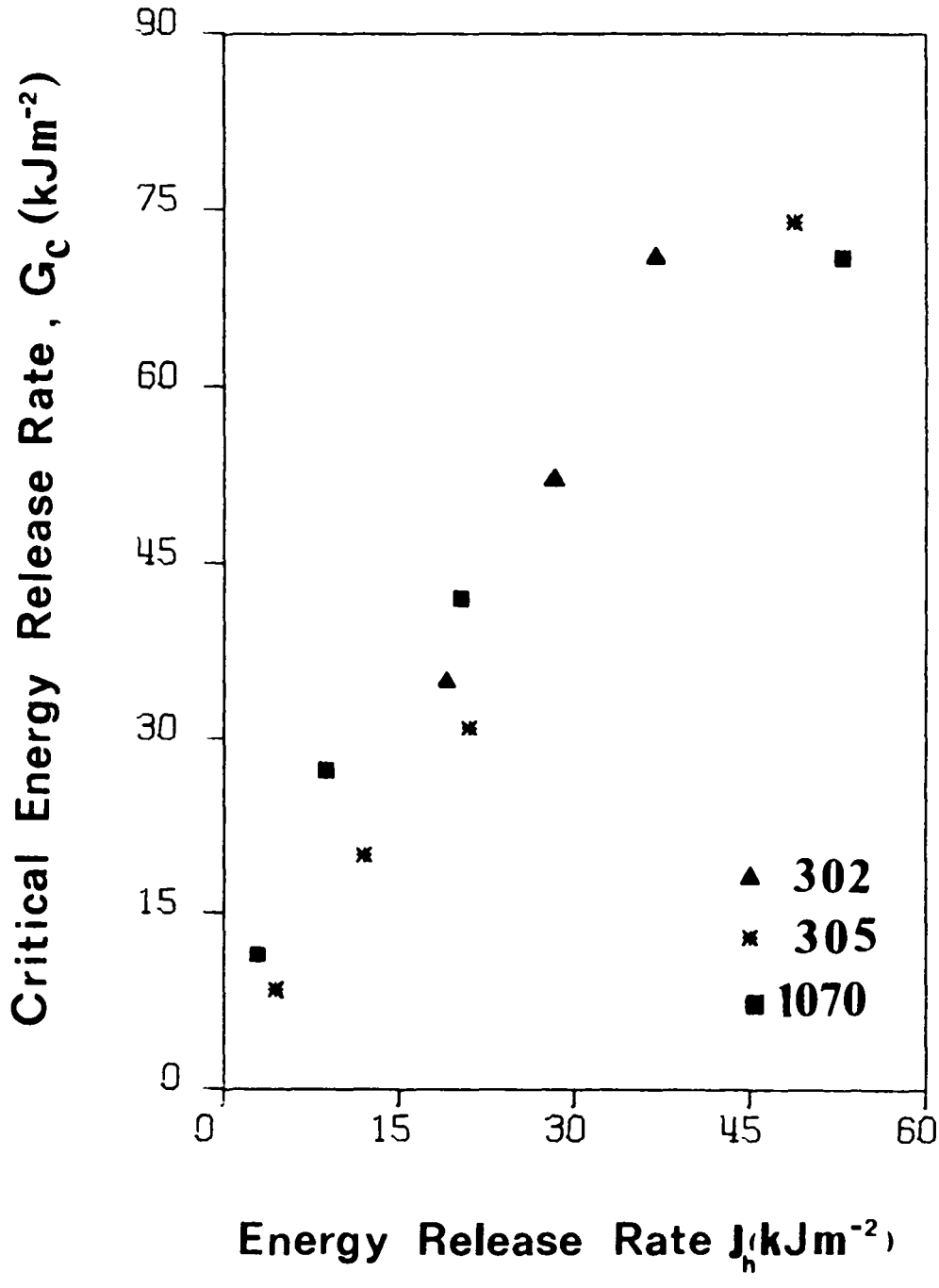

FIGURE 4

Experimental results on fracture toughness in AISI 302 and 305 stainless steel and 1070 carbon steel. Each point on the plot represents the average value of the results of three experiments.

and b is the width of the specimen [18].

The value of J_h is calculated according to the following formula,

$$J_h = \sigma^2_{max} \pi \ell \, F^2(\ell/b)E^{-1}$$

where σ_{max} is the maximum applied stress during the fatigue cycle, ℓ is the length of the interrupted fatigue crack.

The statistical analysis of fracture toughness was conducted for AISI 304 cold rolled, full hard austenitic stainless steel. Figure 5 shows the results of 80 experiments on fracture toughness for that material.

B. Kinetics of CL Propagation

The rate of crack growth for AISI 304 cold rolled, full hard steel under the previously described conditions was plotted as a function of J in Figure 6. After the initial acceleration the crack stopped growing at approximately 8 kJ/m^2, the value of J (see Figure 6). Such a decelaration is an often observed phenomenon. When the decelaration of the crack growth occurs, the damage zone begins to expand. In the literature this phenomenon is called "crack arrest". The damage expansion (formation of an ϵ-zone) associated with the "crack arrest" is shown in Figure 7.

The general views of the well developed crack layers in 301, 304 and 1070 AISI steels are shown in Figures 8, 9 and 10. These pictures explicitly show that crack propagation is accompanied by a surrounding layer of intense 'damage'.

Macroscopic configurations of the CL appear to vary among various materials tested under identical loading conditions. The only parameter with length dimension in the conventional fracture mechanics is $(K/\sigma_y)^2$. The yield stresses σ_y for the tested materials are 780 MNm^{-2}, 920 MNm^{-2} and 590 MNm^{-2}. The experimentally measured non-dimensional parameter r_p/ℓ takes the following values at the 6mm crack length: 0.0341, 0.0476, 0.095. At the same time the theoretical characteristic size $(K/\sigma_y)^2/\ell$ for the considered conditions equal correspondingly 1.6, 1.18 and 1.22. Therefore, K and σ_y are not sufficient to describe the observed phenomena. This discrepancy calls for additional parameter that would reflect differences in the CL growth process on the microscopic level. Such a parameter, damage density ρ, will be introduced in the next Chapter.

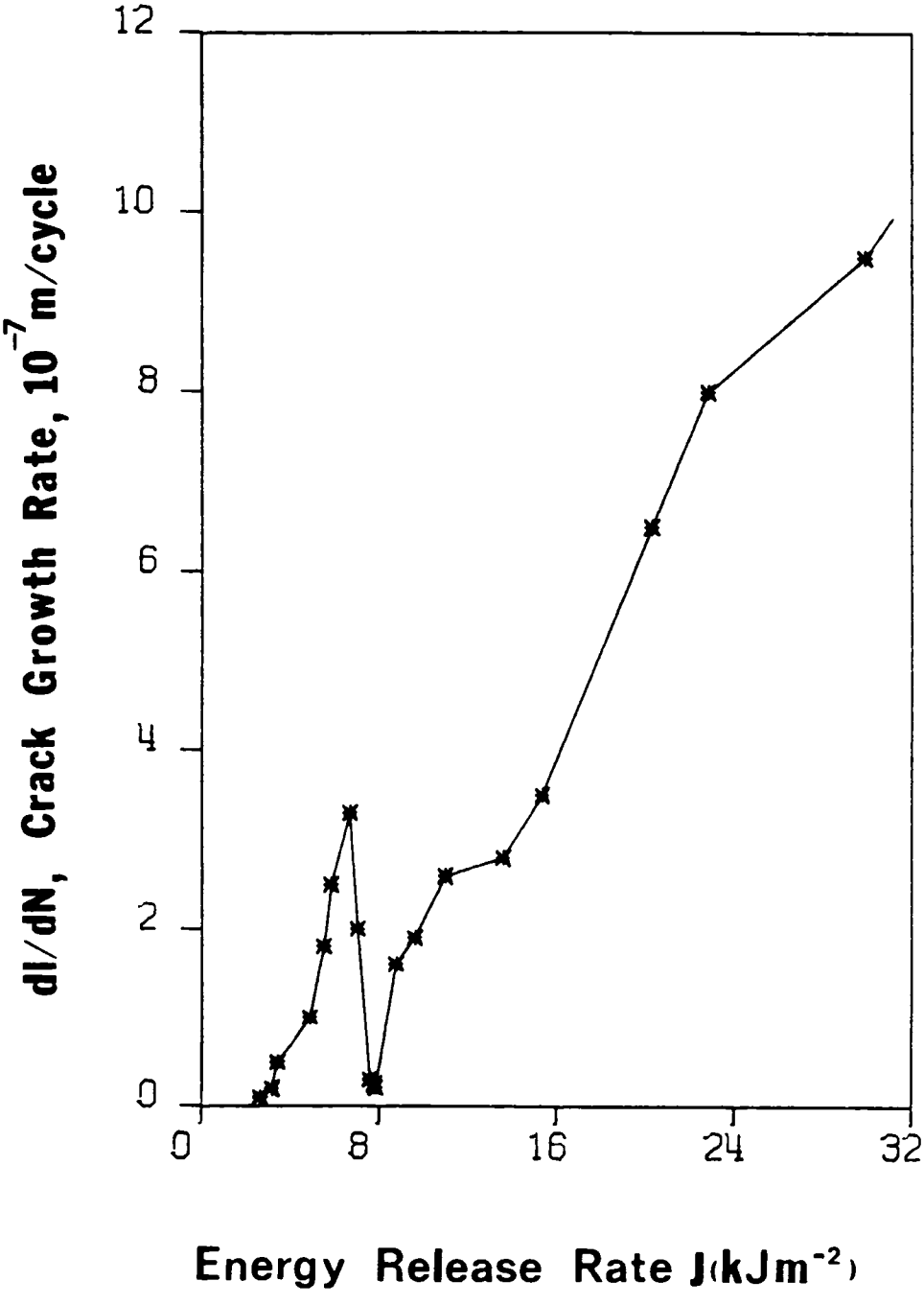

FIGURE 6

Crack growth rate vs. energy release rate in 304 AISI stainless steel. The decelaration part of the curve corresponds to the formation of ϵ-zone.

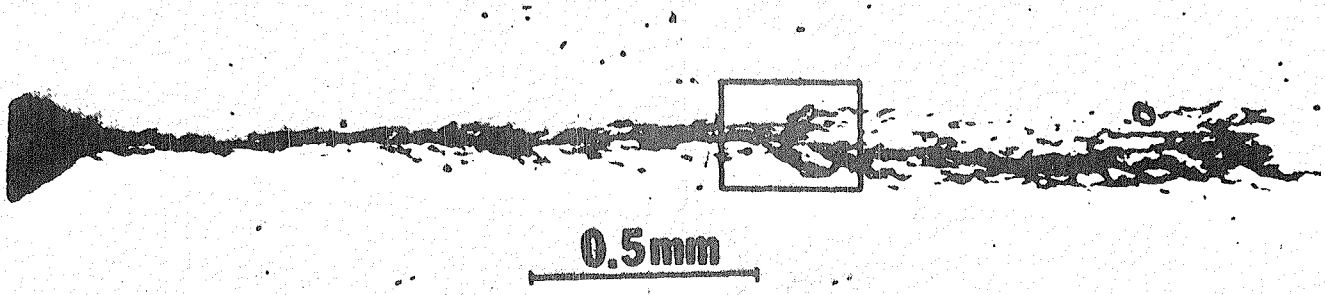

a

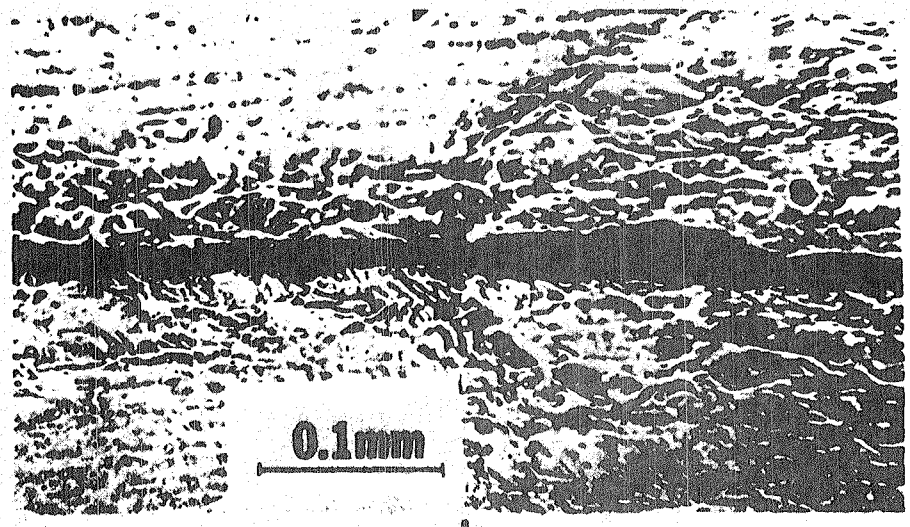

b

FIGURE 7

Pictures of ϵ-zone corresponding to the "crack arrest" phenomenon: (a) general picture of the crack; (b) enlarged area enclosed in the box on Figure (a). This picture is taken in polarized light.

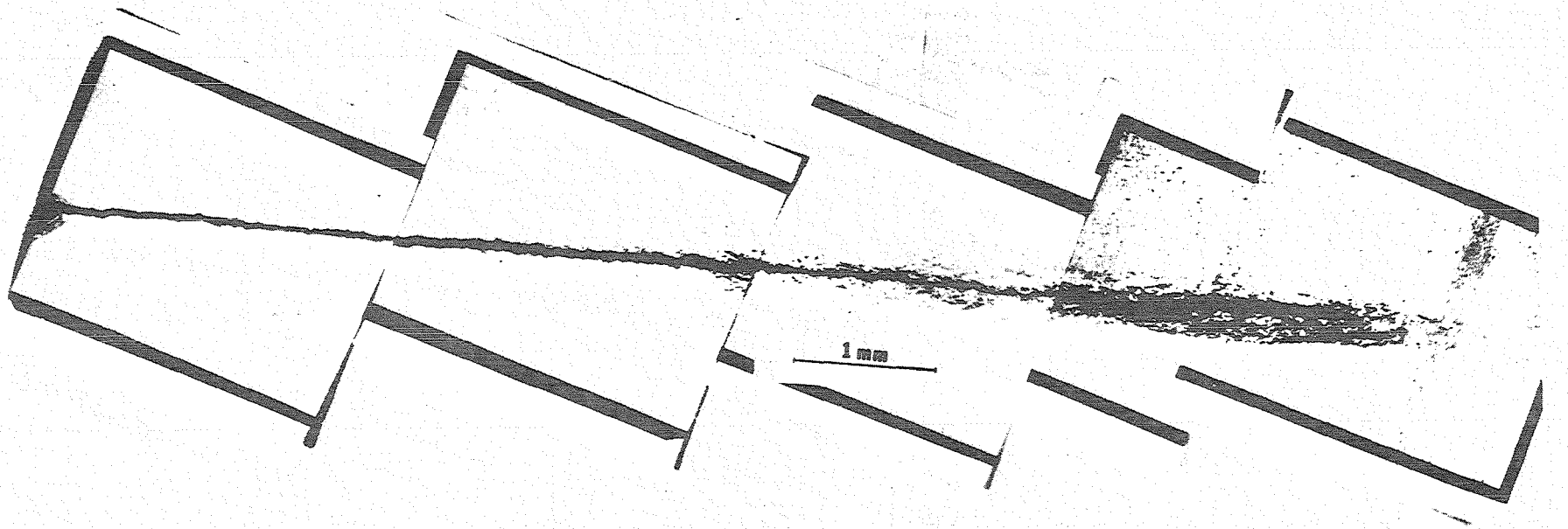

FIGURE 8

Fatigue crack in 0.2 mm thick specimen of 301 AISI stainless steel. Frequency of loading is 50 Hz, max stress is 25% of the yield stress (R = 0.2). Note the damage layer around and ahead of the main crack. Crack length - 9mm.

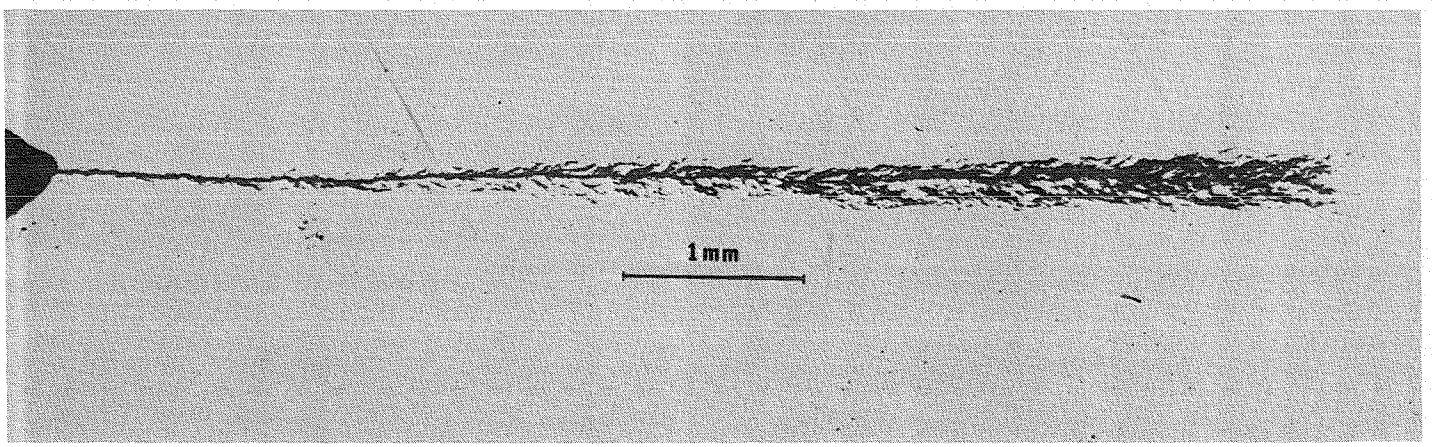

FIGURE 9

Fatigue Crack in 0.15mm thick specimen of 301 stainless steel. Frequency of loading is 50 Hz, max stress is 25% of the yield stress (R = 0.14). Crack length - 7mm.

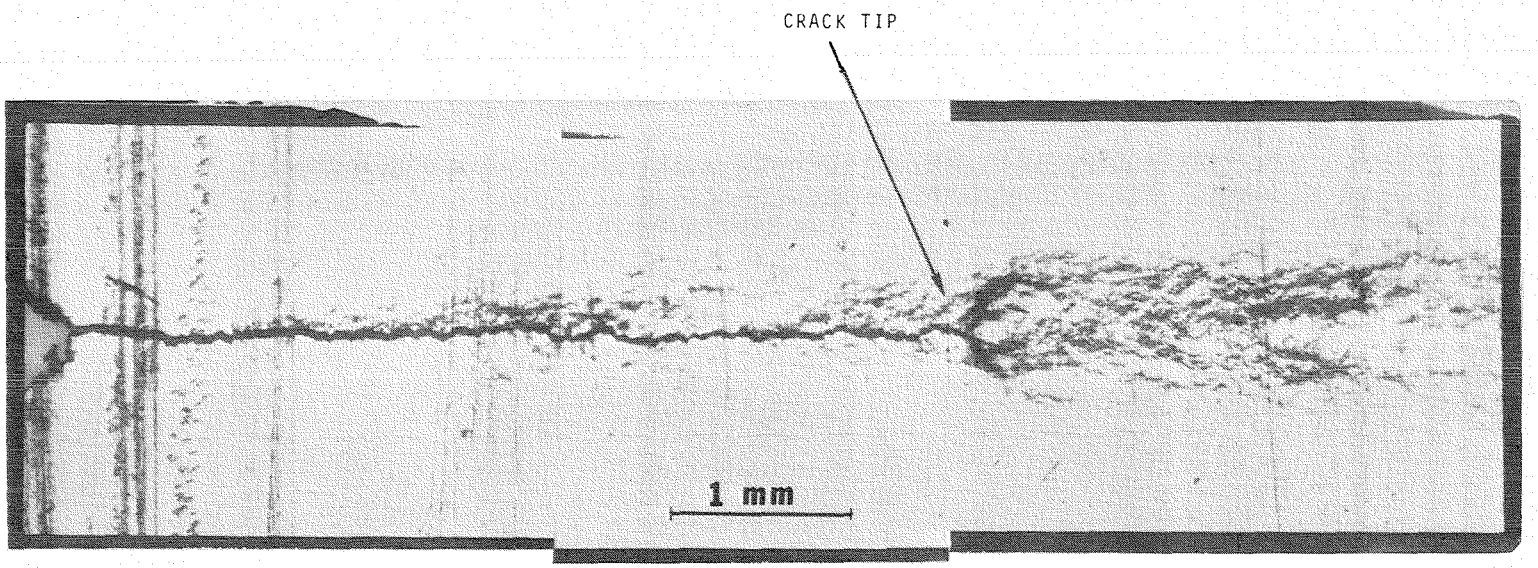

FIGURE 10

Fatigue crack in 0.5mm thick specimen of 1070 AISI steel. Frequency of the loading is 50 Hz, maximum stress is 25% of the yield stress (R = 0.2). Note the damage layer around and ahead of the main crack. Crack length - 7mm.

C. Morphology of Crack Layer

If the damage is viewed on a progressively finer scale a hierarchy of defects can be visualized. At low magnification nonhomogeneous deformation of continuous media is observed; no discrete defects could be identified (Figure 11). In Figure 12 the traces of discontinuous surfaces, which correspond to slip band extrusions and intrusions, are clearly observed in 304 AISI stainless steel. Further magnifications of the object shown in Figure 12, which is seen as a single line, show that it represents on average 20 discontinuous surfaces (Figures 13a and 13b). If we are to continue to view the damage at the progressively higher resolutions the following elements could be observed: clusters of dislocations, single disloctions, subgrain boundary precipitates, point and lattice defects. In this paper two types of defects were considered and the energy dissipation associated with these were estimated.

The first type of defect to be investigated is the distribution of dislocations around the crack tip since dislocations are commonly associated with the plastic deformation. In Figure (14) the map of dislocation density $_{disl}$ around the fatigue crack based on the measurements of microhardness is shown. In order to plot this map the following relationship between the microhardness (DPH) and dislocation density ρ_{disl}, obtained on the basis of [19,20,21] was used:

$$\rho_{disl} = \sqrt{\frac{DPH - C_1}{C_2}} \qquad (3)$$

where C_1 and C_2 are experimentally obtained constants. A three-dimensional picture of dislocation density around fatigue crack is shown in Figure 15.

The discontinuity surfaces represent the second type of defects under

consideration. A statistical analysis of the discontinuities was done according to the methodology described in Section II B.

The discontinuity surface density ρ_{disl} is introduced by the formula [16,17]

$$\rho_{disl} = 2P_L \frac{mm^2}{mm^3} \qquad (4)$$

where P_L is the number of point intersections per unit length of test line. The density of discontinuity surfaces changes from 10^1 to 10^5 mm^2/mm^3 at the observable regions. A map of the discontinuity distribution based on this methodology is shown in Figure 16.

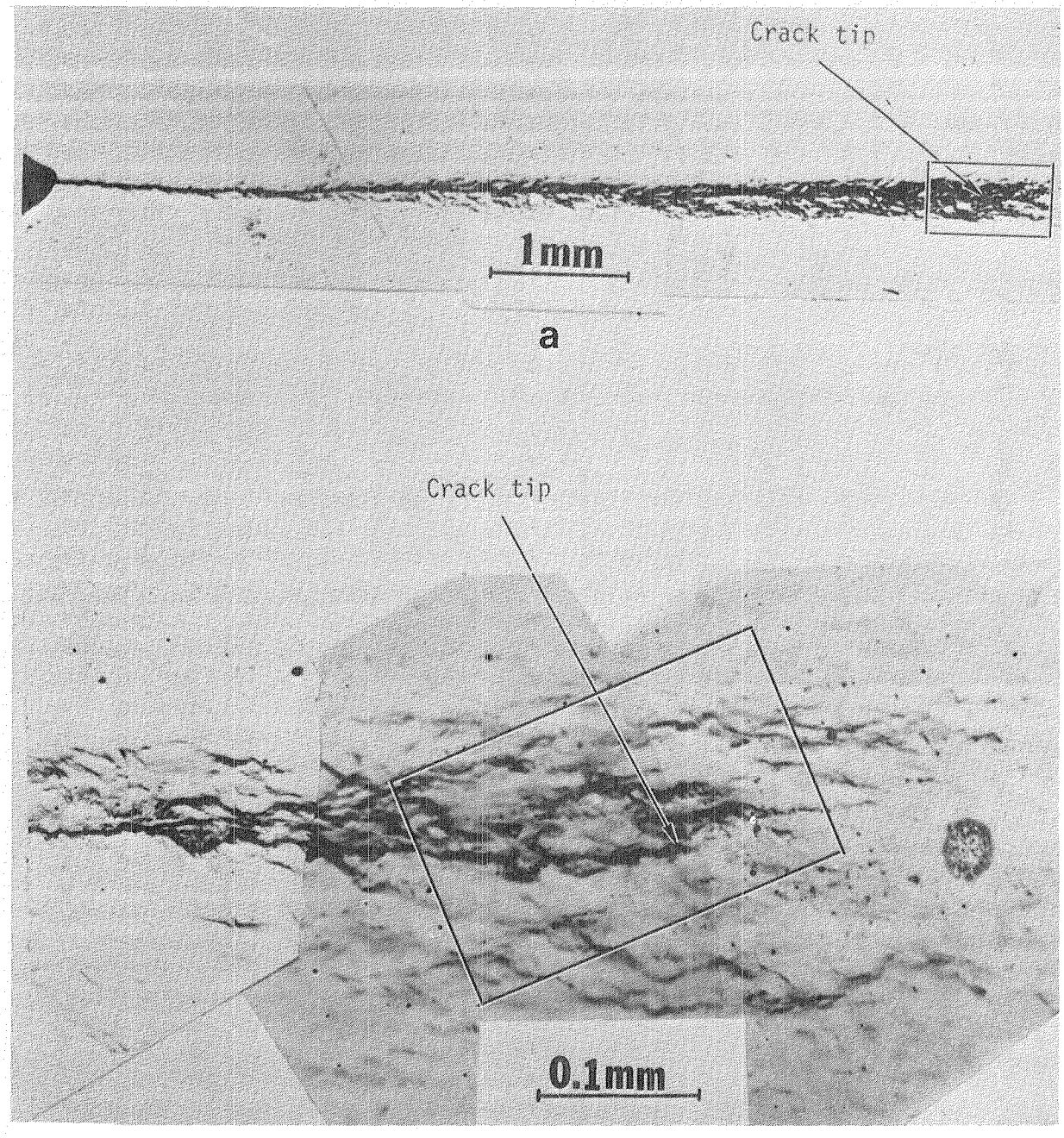

FIGURE 11

Morphology of crack layer at different magnifications: (a) General view of the fatigue crack at low magnification; (b) The crack tip region enclosed in the box on 11a. Extensive damage is seen around and in front of the crack tip. The features of an element of "damage" become clearer under higher resolution (see Figure 12).

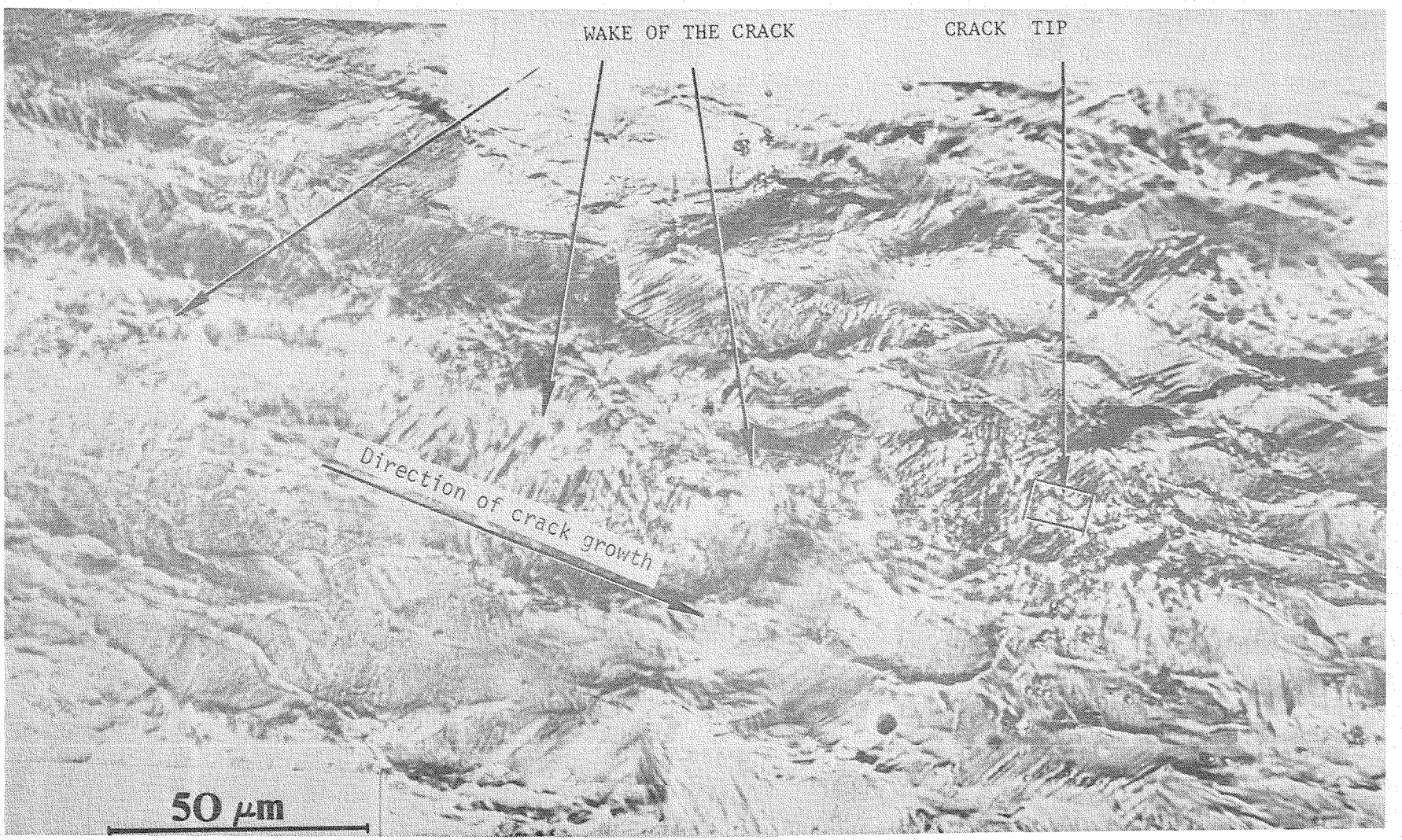

FIGURE 12

Picture of the crack tip region enclosed in the box shown in Figure 11b. Extensive damage consisting of slip band intrusions and extrusions is clearly observed. The arrows indicate position of the wake of the crack. The crack itself is out of focus because the focusing was aimed at the slip bands. Pictures at this magnification were used for statistical evaluation of discontinuity density ρ around the crack. The finer structure of the slip bands enclosed in the box become clearer under higher resolution (See Figure 13a).

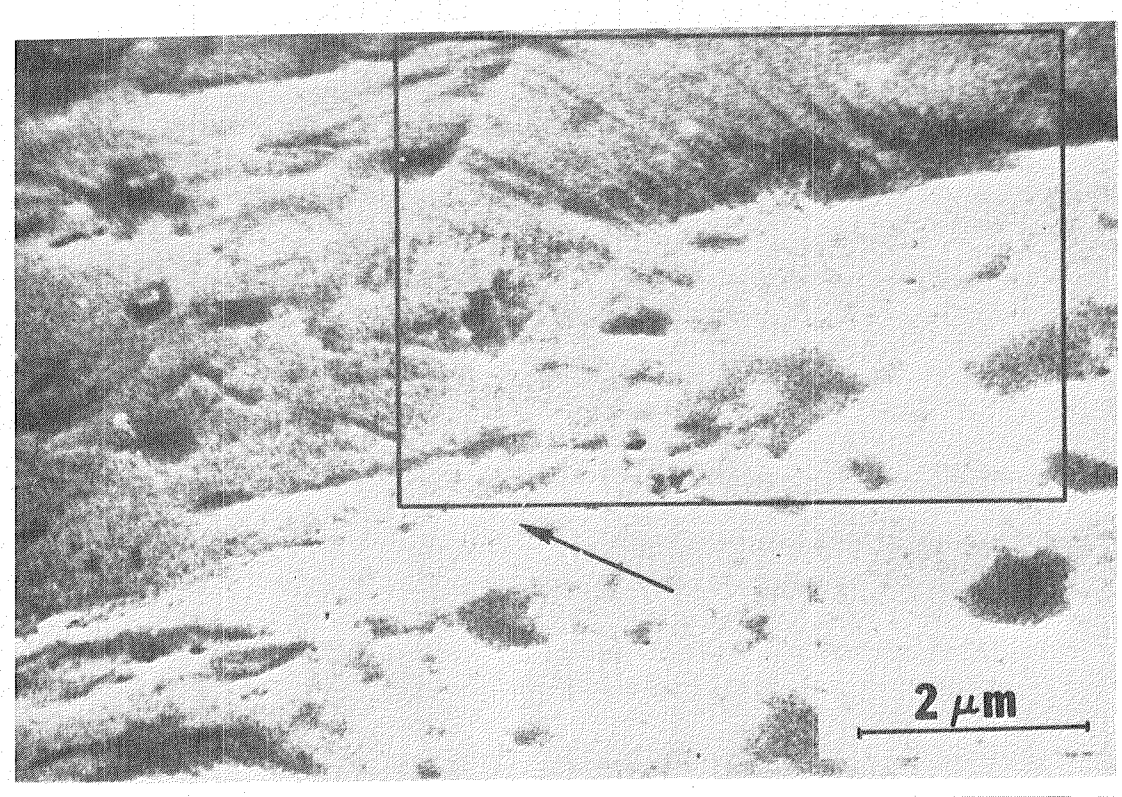

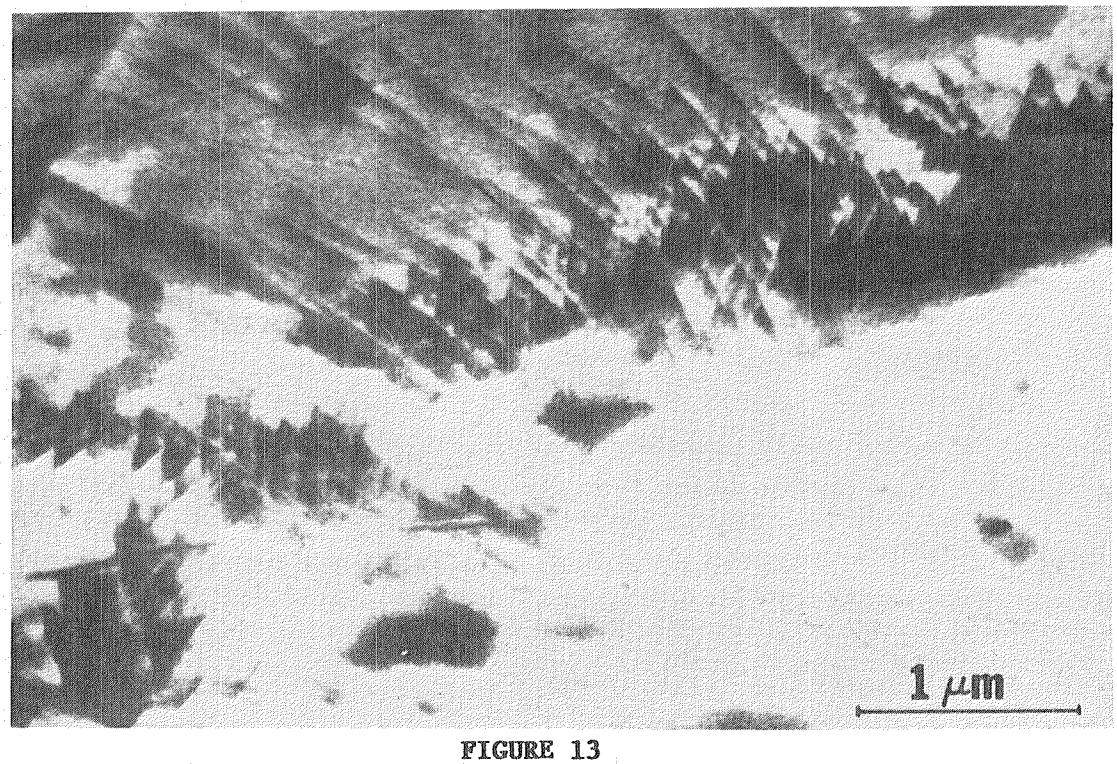

FIGURE 13

SEM pictures of the crack tip region taken at 10,000 and 20,000 magnifications. The crack tip is shown by the arrow in Figure a. In Figure b the region enclosed in the box in Figure a is magnified. The traces of the discontinuity surfaces are clearly visible.

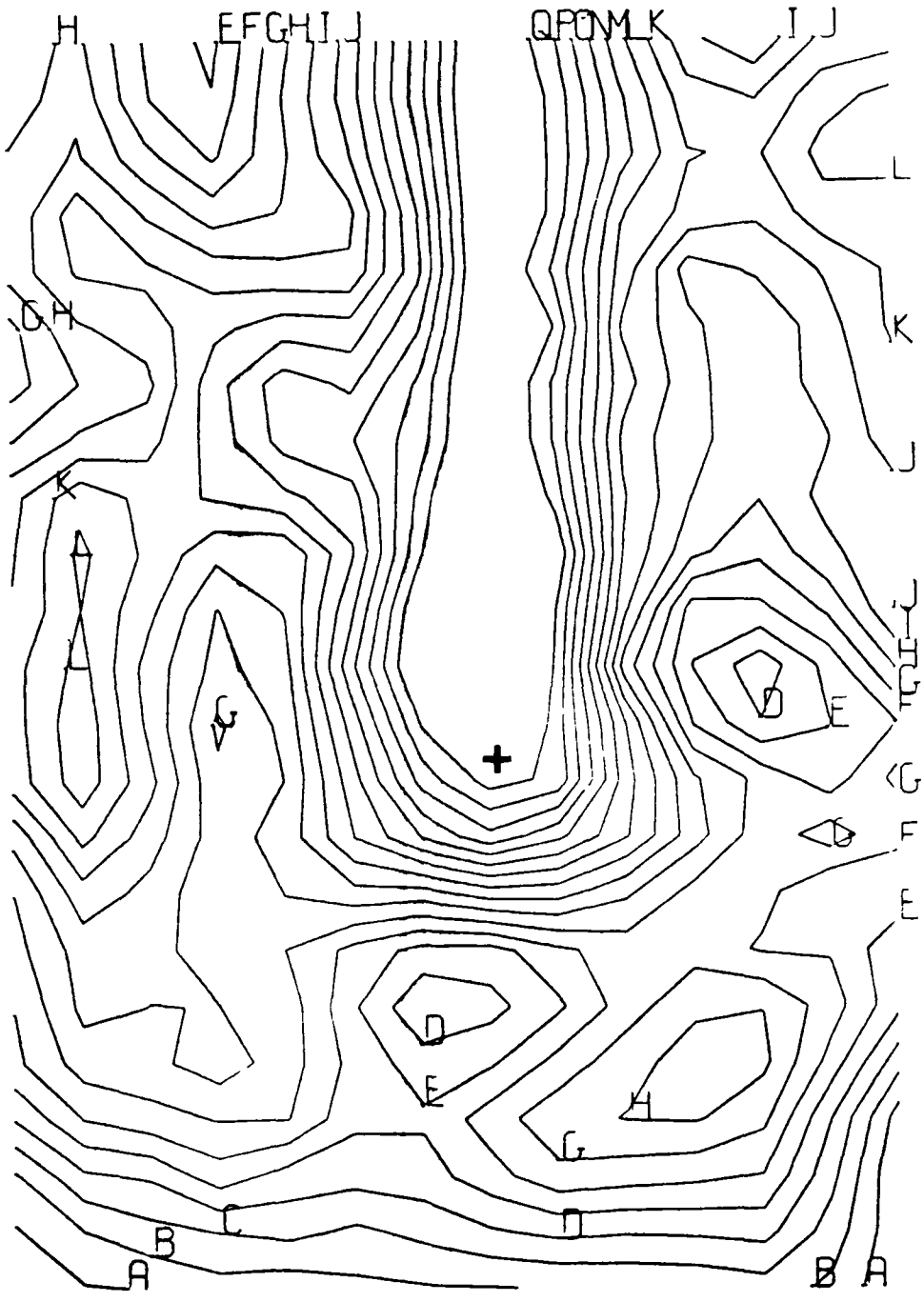

FIGURE 14

Contours of equal levels of dislocation density around the crack tip in 304 AISI stainless steel. Contour A corresponds to the dislocation density 10^7 cm^{-2}. B=A+d, C=A+2d, D=A+3d, Q=A+19d, where d=5.10^7 cm^{-2}. Symbol "+" indicates the crack tip.

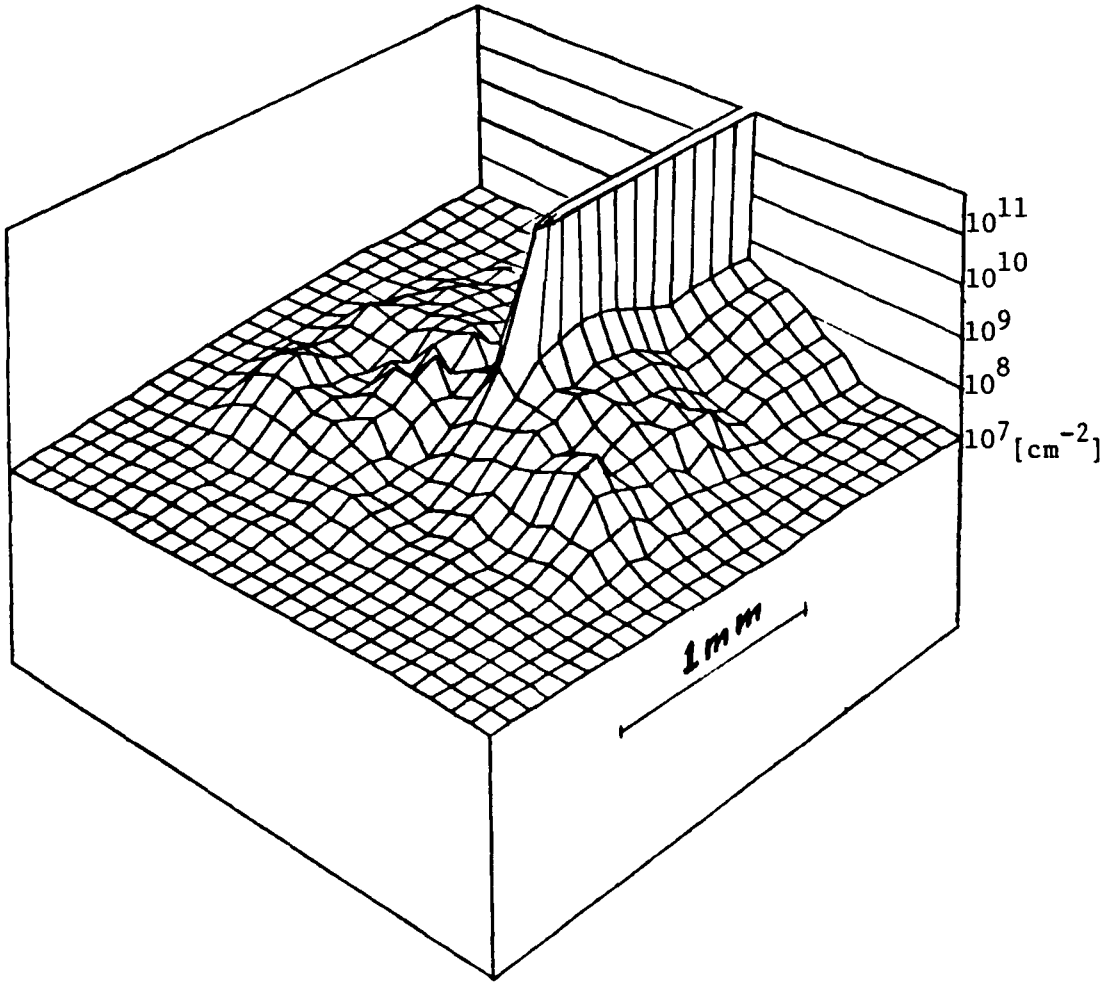

FIGURE 15

Three dimensional picture of dislocation density $\rho[\frac{cm}{cm^3}]$ around the fatigue crack in 304 AISI stainless steel. Sample No. 174. Crack length - 7mm.

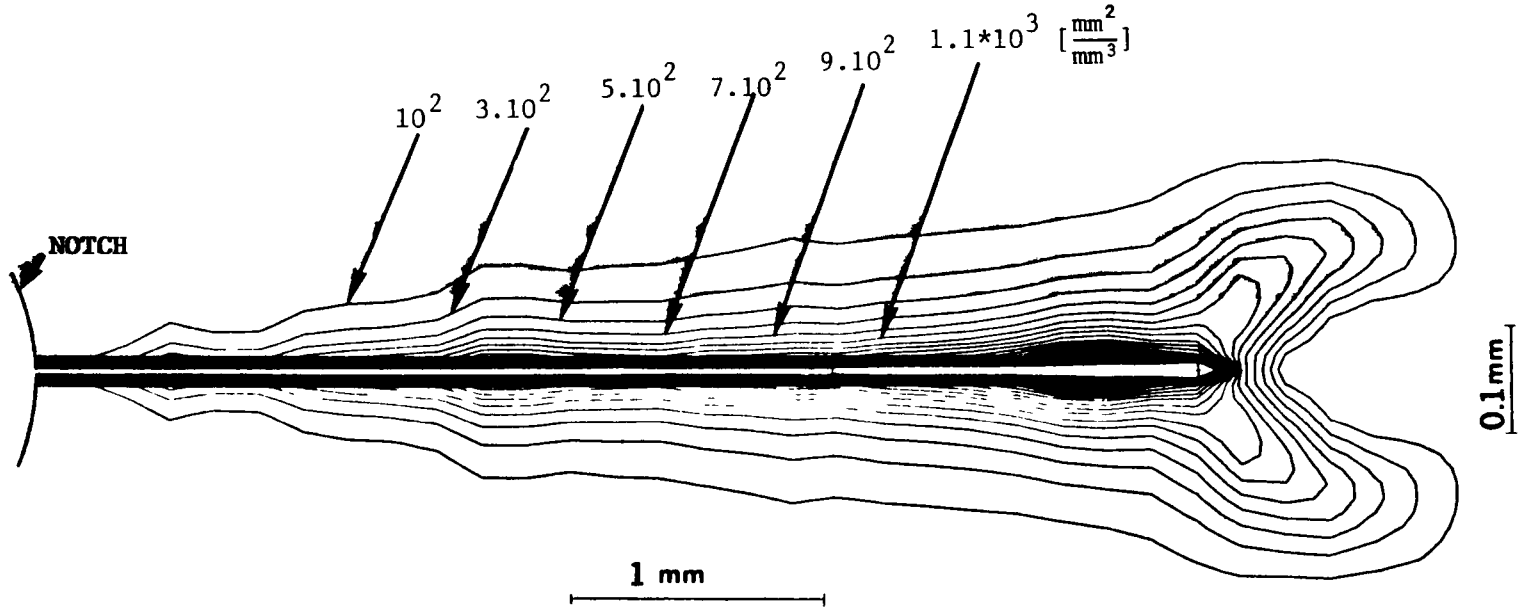

FIGURES 16

The countours of equal levels of discontinuity density $\rho[\frac{mm^2}{mm^3}]$ around the fatigue crack in 304 AISI stainless steel. Symbol "+" indicates the crack tip.

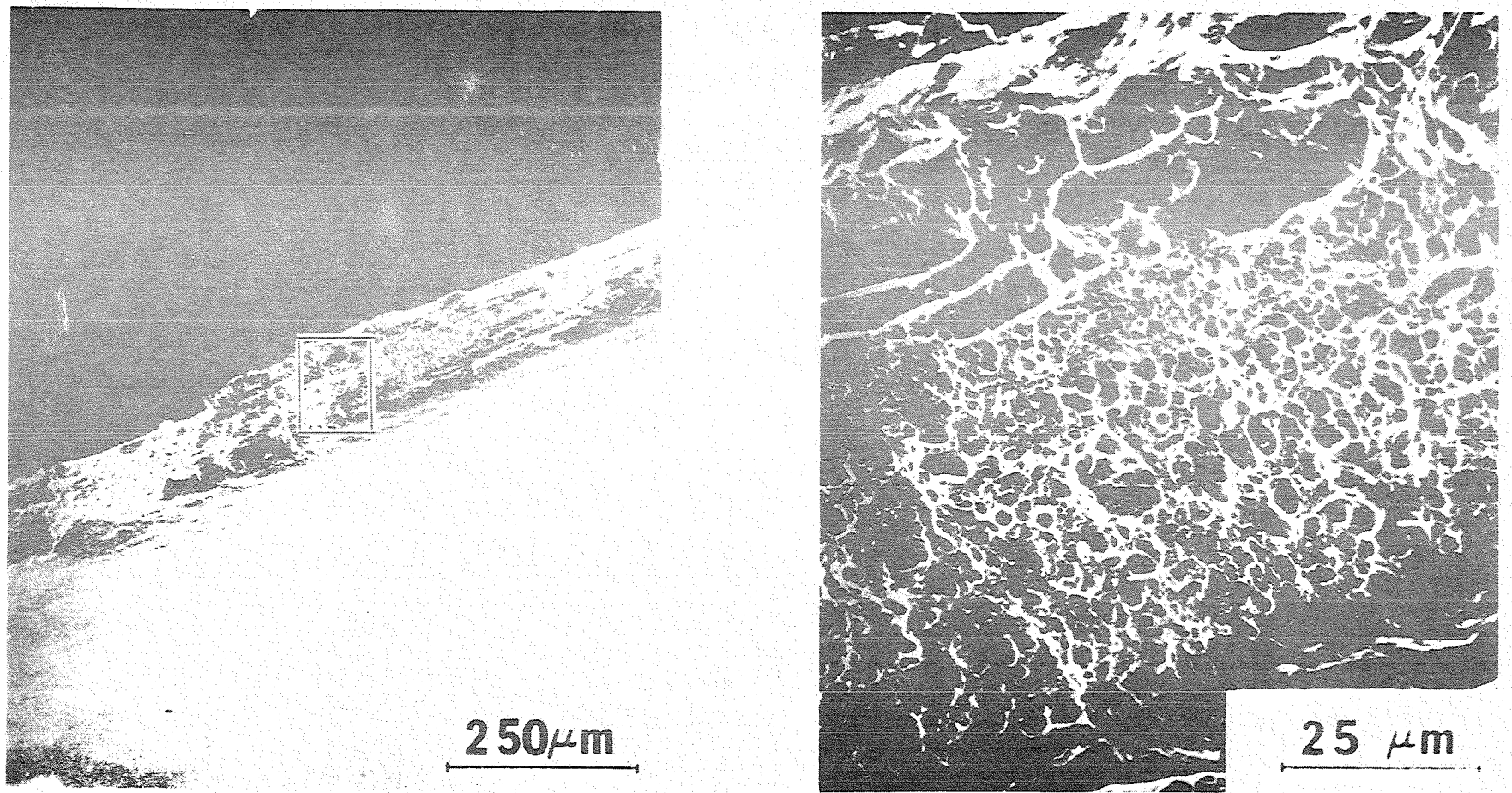

FIGURE 17

SEM pictures of fracture surface of AISI 304 stainless steel (a) region of brittle-ductile transition, (b) voids on the fracture surface show typical ductile failure.

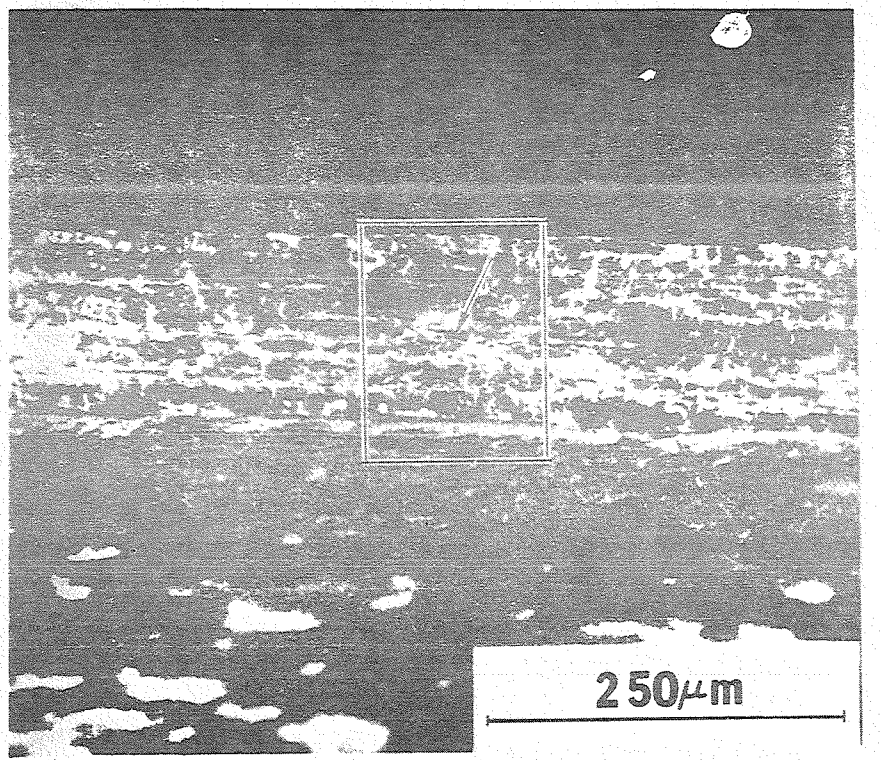

a

Microcracks are oriented along the direction of crack propagation.

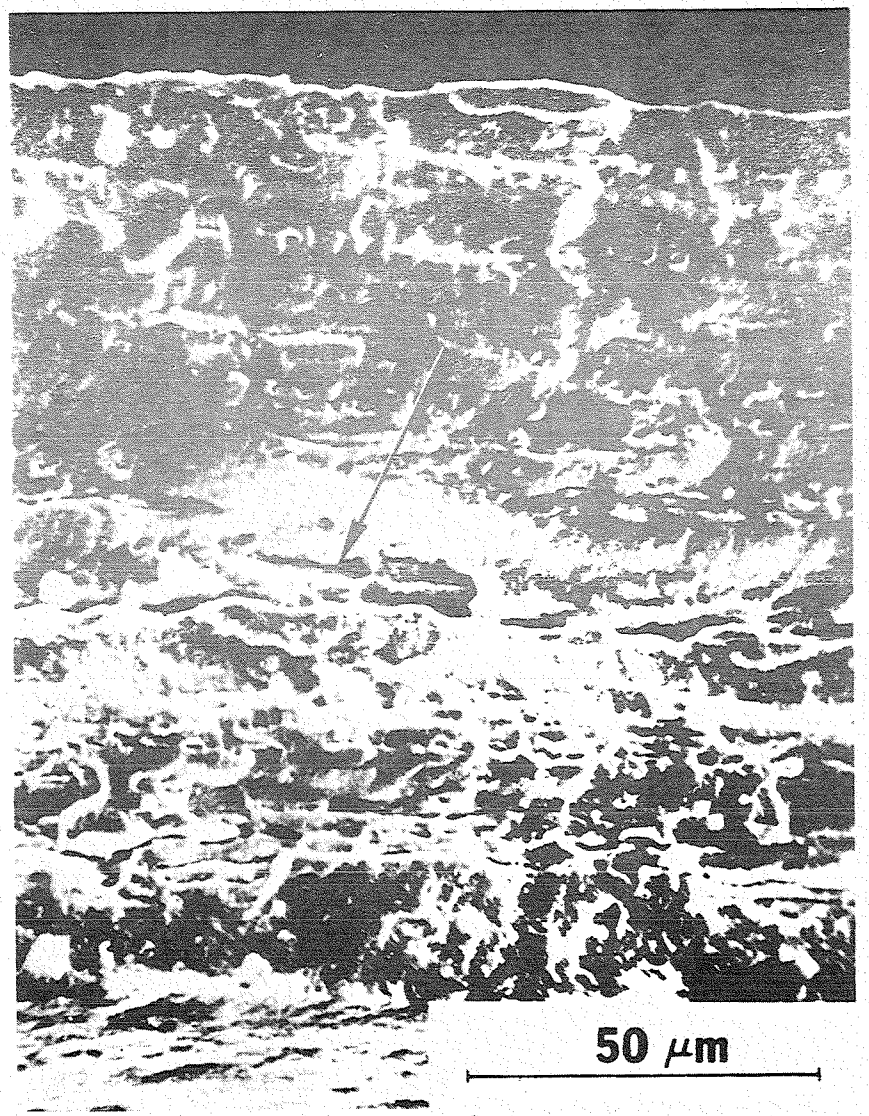

b

Enlarged region of the area enclosed in the box in Figure a. The surface has a typical brittle fracture appearance.

FIGURE 18

Region of the quasistatic crack growth in AISI 304 stainless steel. The arrows indicate the typical microcrack propagation in the direction of the main crack.

CHAPTER IV

DISCUSSION

Our results show that the critical energy release rate G_c depends on the methods employed in the preparation of the specimen for the fracture toughness test. This agrees with the results of other workers. A statistical analysis of the data from Figure 5 is presented on Figure 19.

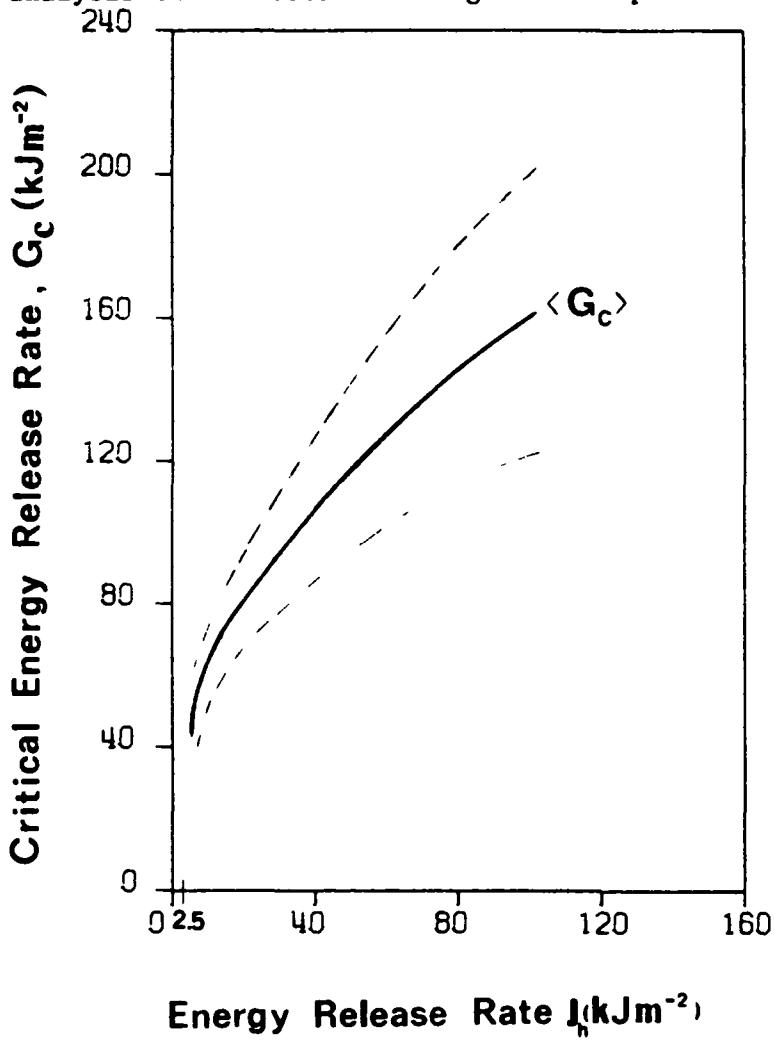

FIGURE 19

Critical energy release rate G_c as a function of the energy release rate J_h. Solid line represents the average values of G_c. Dashed lines indicate the 63% confidence zone. This plot is result the of statistical evaluation of the data shown in Figure 4. The value of $2.5 kJm^{-2}$ corresponds to minimal crack length.

A mathematical expectation is shown by the solid line and the 63% confidence zone is shown by the dotted lines.

As illustrated by this plot, the average energy release rate G_c increases with the increase of J_h. It is important to note that the variance of G_c also increases with the increase of J_h. The latter is an important factor for engineering design applications.

In this study we observed nonmonotonic crack advance under monotonic changes of energy release rate J. There is an apparent alternation between the crack advance and damage growth processes. This implies the existence of intrinsic properties of the fracture process which are not reflected by the J integral.

The monotonic crack growth as well as the dependence of G_c and its variance on the history of the process call for an explanation in terms of the morphologic changes accompanying the crack propagation. One possible explanation is given in the CL theory.

A. Concept of Crack Layer

CL is represented schematically in Figure 20.

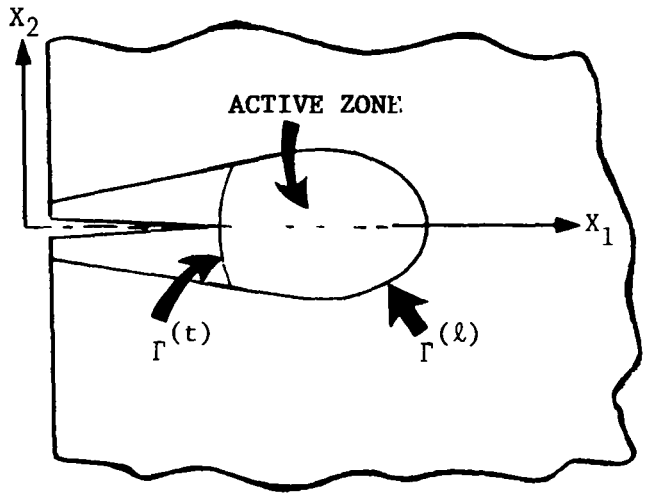

FIGURE 20

Sketch of crack layer.

The zone surrounding the crack where $\rho>\rho_0$ (where ρ_0 is the reference level of damage) is called crack layer. The active and wake zones are distinct in the following. The active zone where the damage growth takes place ($\rho>\rho_0$, $\dot{\rho}>0$ where $\dot{\rho}$ is a rate of damage growth) is bound by the leading and trailing edges $\Gamma^{(\ell)}$, $\Gamma^{(t)}$. The wake zone can be described as the trace of the active zone movement and characterized by $\rho>\rho_0$, $\dot{\rho}=0$. We are considering only two elementary movements of the active zone: translation as a rigid body and isotropic expansion (the spread of damage),

$$v_k(x) = v_k(x^o) + \dot{e}(x-x_k) \tag{5}$$

where v_k is a rate of the translation of the center of the ative zone x^o, $x-x^o$ is a radius vector for arbitrary point of the active zone, $\dot{e}$ is a rate of isotropic expansion. (We look upon the distribution of defects as a mass distribution and the center of the active zone is found as a center of mass.)

The measure of isotropic expansion 'e' is given by the logarithmic measure

$$e = \ln d/d_o \tag{6}$$

where d is a characteristic size of the active zone and d_o is that size in the initial configuration.

For rectilinear CL growth

$v_1 = \dot{\ell}$ - rate of crack length growth

$v_2 = 0.$

Then according to the CL theory the rates of extension ($\dot{\ell}$) and expansion ($\dot{e}$) are given as

$$\dot{\ell} = \frac{\beta_1 \int_0^{\ell} J(\ell)d\ell}{\gamma R_1 - J_1(\ell)} \tag{7}$$

and

$$\dot{e} = \frac{\beta_1 \int_0^{\ell} J(\ell)d\ell}{\gamma R_o - M} , \qquad (8)$$

where J, and M are the well known path independent integrals:

$$J = |J_1|, \qquad J_1 = \int_{\Gamma(\ell)} [f_\varepsilon \cdot n_1 - \sigma_{ij} n_j u_{i,1}]d\Gamma; \qquad (9)$$

$$M = \delta_{k\ell} \int_{\Gamma(\ell)} [f_\varepsilon n_k x_\ell - \sigma_{ij} j_j u_{i,k} x_\ell]d\Gamma ; \qquad (10)$$

the resistance moment

$$R_1 = \int_{\Gamma(t)} \rho \cdot n_1 d\Gamma , \qquad (11)$$

stands for a measure of resistance of the crack extension, and

$$R_o = \int_A \rho \, dA, \qquad (12)$$

is a measure of resistance for crack expansion.

Above f_ε, n_k, σ_{ij} and u_i stand for strain energy density, k-th component of the unit normal vector with respect to a contour Γ, stress tensor components, and displacement vector component correspondingly. "," stands for the derivative with respect to x_1, and $\delta_{k\ell}$ is a Kroneker's delta. From the Equation (7) the rate of crack growth becomes uncontrolled ($\dot{\ell} \to \infty$) when J_1 approaches R_1. Thus, conventional G_c could be identified with R_1:

$$R_1(\ell^*) = G_c. \qquad (13)$$

Therefore, history dependency of G_c corresponds to the evolution of the resistance moment R_1. The density damage can be represented as

$$\rho = R_1^* \delta(x_2) + \rho(x_2) \quad , \qquad (14)$$

where R_1^* stands for core of damage associated with the crack edges and their immediate vicinity (boundary layer), $\delta(x_2)$, the Dirac's delta function which indicates that the core of damage R^* is concentrated on the crack trajectory ($x_2 = 0$) and $\rho(x_1,x_2)$ stands for the measured damage distribution outside of core of damage.

Integrating both sides of Equation (14) over the trailing edge $\Gamma(t)$ we find:

where $\tilde{R}_1$ is the variable part of the resistance moment.

In the regions where fracture surface has the same appearance one would expect the core of damage R_1^* to be the same.

The fractographic analysis of the fracture surfaces shows no changes in the fracture appearance in the region of the quasi-static crack growth. Therefore, we assumed R_1^* to be a constant. The value of this constant is associated with microcracks indicated on Figure 18. Study of the sizes, orientation and density of these microcracks for quantitative evaluation of R_1^* is under way.

According to the equations (13) and (15) the critical value of G_c can be resolved into two parts: G_c associated with the core of damage R_1^* and $\tilde{G}_c$ associated with the damage dissemination around the crack,

$$G_c = G_c^* + \tilde{G}_c \qquad (16)$$

The damage density G_c introduced above represents either dislocations or discontinuity surfaces, or any other type of defect or their superposition.

The value of G_c is measured in the conventional fracture toughness evaluation (macroscopic) test. On the other hand, according to the CL theory, G_c can be evaluated in terms of the integral damage R_1 obtained from microscopic analysis the and specific enthalpy γ of damage under consideration. The comparison of the two values of G_c will reveal the weight of each particular defect in the fracture process. Following this argument two types of defects, namely dislocations and discontinuity surfaces, are considered.

B. Evaluation of Energy Stored in the Dislocation Network

Energy E_{disl} of one dislocation could be estimated as 10-20 nJ/m [22]. When the dislocation network is generated the energy associated with dislocations per unit crack increment is

$$E = E_{disl} R_1$$

Figure (14) shows the map of the dislocation distribution in the vicinity of the crack tip.

Resistance moment R_1 for the map shown in Figure (14) is $R_1 \sim 10^{10}\ m^{-1}$. Then the energy stored in the dislocation network

$$E \sim 10^{-8}\ J/m * 10^{10}\ m^{-1} = 10^{2}\ J/m^{2}$$

constitutes 0.1% from the experimentally measured critical energy release rate $G_c = 120\ kJ/m^2$. It is worth noting that the more appropriate procedure would involve consideration of the entire dislocation network since it has been established that there is a definite stage of dislocation density saturation for a given steel ($10^{12}\ cm^{-2}$). But, even this will not change much the estimated value of E.

If we consider the case when the maximum dislocation density ($10^{12}\ cm^{-2}$) is everywhere in the CL, the full energy of dislocation network will not be higher than 1% of the G_c value. Therefore, the generation of dislocations can explain neither the value of G_c nor the evolution of G_c with

crack advance. We conclude that such a simplistic dislocation approach cannot account for actual values of critical energy release rate G_c.

C. Evaluation of Energy Associated With the Discontinuity Surfaces

The integral cross-section damage R_1 for 304 AISI steel was experimentally obtained according to the methodology and formula (Eq. 11) given above. Using the method of least squares the functional relationship between R_1 and J_h is found and plotted in Figure 21 as a solid line, stars represent experimental data. The experimental data on fracture toughness (Figure 5) are replotted in Figure 22 as G_c vs. $\tilde{R}_1$.

The specific energy of a discontinuity surface is presented by the slope of the solid line (which is in its turn obtained by the least square method).

Assuming the average thickness of the slip lines (layers) to be $\delta = 50\text{Å}$ and mass density $d = 8\ g/cm^3$, one can obtain the total mass $\tilde{R}_1$ of damaged material per square centimeter of crack surface:

$$\tilde{R}_1 = R_1 \delta d = 10^{-2}\ g \cdot cm^{-2}$$

The ratio $G_c/\tilde{R} = \tilde{\gamma}$ represents the specific energy of damage $(4.10^9 . erg.g^{-1})$ which is the same order of magnitude as the heat of fusion of steel $(2.9.10^9\ erg.g^{-1})$ [23]. This result indicates the relationship between fracture and a phase transition. The relationship between the processes of fracture and melting (and/or dissociation) was noted first by Born [24] and then was experimentally studied by Born and Furth [25, 26].

Following Born's idea the physical interpretatin of fracture and plastic deformation as an anisotropic localized phase transitions is discussed in [27].

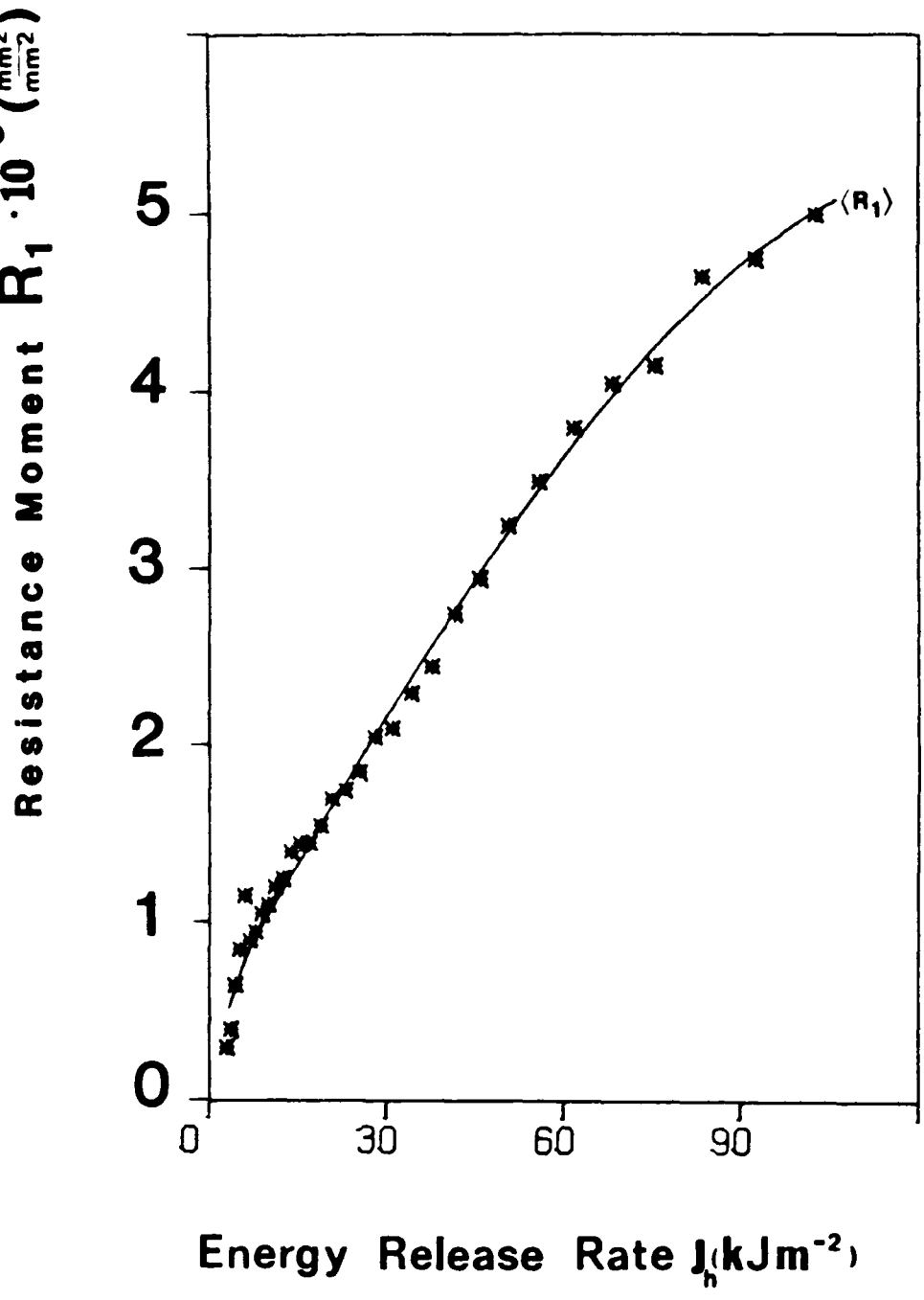

FIGURE 21

Resistance moment R_1 vs. energy release rate. Stars represent calculated values of R_1 from experimentally measured density of damage. The solid line stands for the least square approximation of R_1 dependency on J.

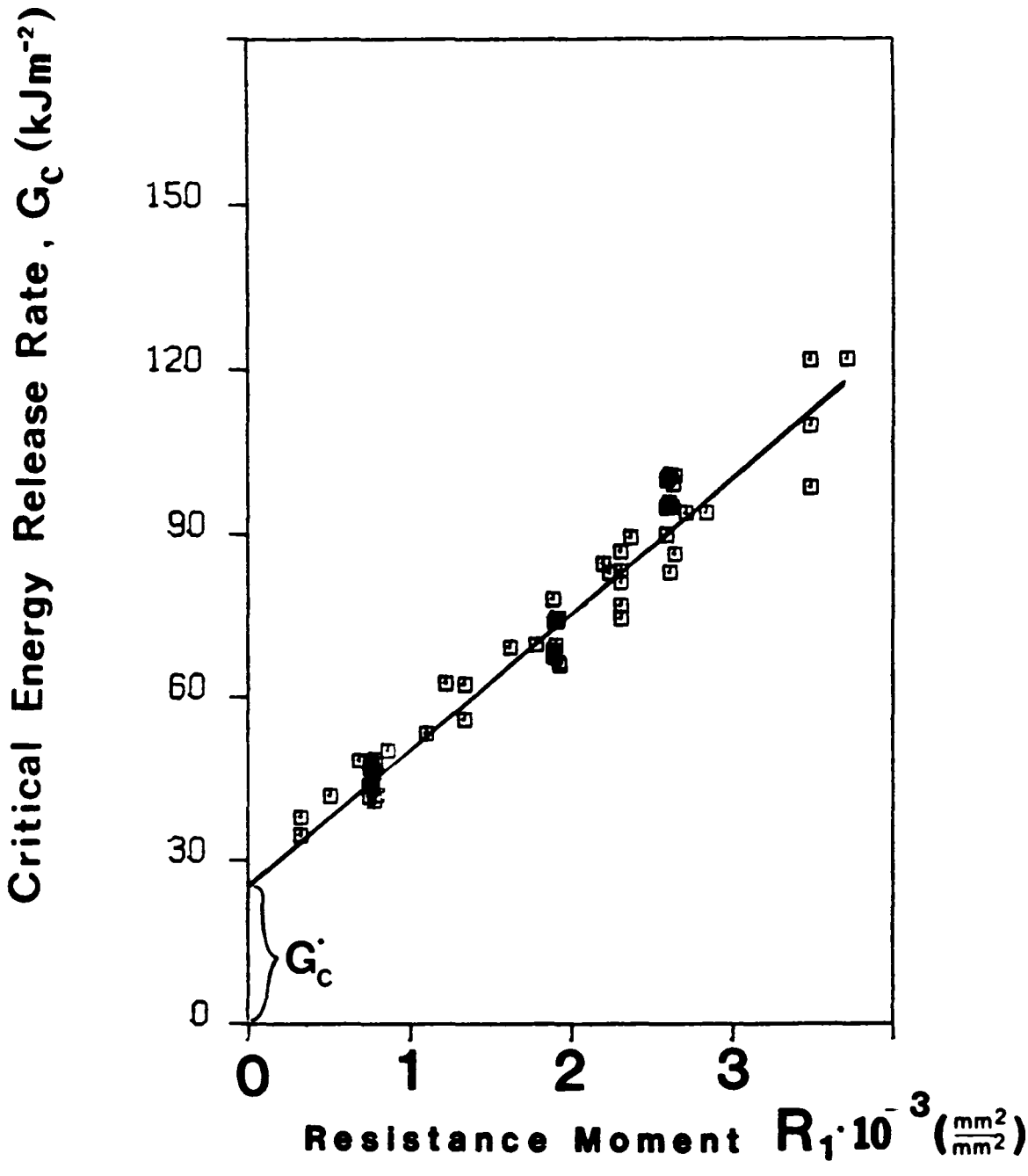

FIGURE 22

Critical Energy Release rate vs. Resistance Moment R_1. Solid line represents the average value of Gc.

CHAPTER V

CONCLUSIONS

1. We confirmed the history dependence of G_c as well as the variance of G_c for the considered loading history.

2. The experimental observations are in favor of the representation of G_c as a product of the specific energy of damage (which is a material constant according to CL theory) and the integral cross-section damage R_1 (history-dependent parameter)

$$G_c = R_1 \gamma^*$$

3. Determination of the major energy sink within the hierarchy of defects is the critical step for the evaluation of the integral cross-section damage R_1. According to our estimation, dislocations can not account for observed G_c values. For AISI 304 stainless steel, the slip band extrusions and intrusions are the candidates for being the major energy sink in plane stress fatigue.

4. Our estimation of the value of specific energy appear to be in the range of the heat of fusion, in accordance with the discussed similarity between fracture and melting (and/or dissociation) processes.

5. The shape of the crack layer (Figure 16) is similar to the plastic zone in the plasticity is helpful in the analysis of stress and strain and, consequently, for the calculation of J and M integrals. However, this is only part of the problem. The resistance moments R_1 and R_o cannot be calculated on the basis of plasticity.

6. The crack arrest phenomenon is related to the active zone shape change. This transition calls for the definition of constitutive equations for (rate of extension) and $\dot{e}$ (rate of expansion).

CHAPTER VI

REFERENCES

1. A. Thompson, "Work Hardening in Tension and Fatigue", A. Thompson ed., AIME, 1975.

2. G. Ghalant and L. Remy, Mater. Sci. Eng., 50 (1981) 253-261.

3. W. Pompe, H. Bahr, G. Gille, W. Kreher, J. Mat. Sci. 13, (1978) 2720-2723.

4. W. Gerbeirich, P. Hemmings, V. Zackay, E. Parker, Fracture 1969, Ed. by P. Pratt, Chapman & Hall, London, 1969.

5. J. Moteff, Proceedings of Damage Workshop, University of Cincinnati, May, 1980.

6. G. Hahn, R. Hoagland, A.Rosenfield, Met. Trans., Vol. 3, 1972.

7. A. Chudnovsky, Proceedings of Damage Workshop, University of Cincinnati, (May, 1980).

8. V. Khandogin and A. Çhudnovsky, "Dynamics and Strength in Aircraft Construction", Editor L. Kurshin, Novosibirsk (1978).

9. A. Chudnovsky, "Crack Layer Theory", NASA Report (to be published).

10. J. Knowles and E. Sternberg, Arch. for Rational Mech. and Analysis, Vol. 44, No. 3, 1972.

11. D. Curran, L. Seaman, A. Shockey, Physics Today, Jan., 1977.

12. P.A. Jacquet, Met. Rev., 1956, Vol. 1, Part 2.

13. Bathias and R. Pelloux, Metallurgical Transactions, Vol. 4, May 1973, 1265-1273.

14. E. Exner, J. Pickens, J. Gurland,Metallurtgical Transactions, Vol. 9A, 736.

15. H. Cramer, Mathematical Methods of Statistics, Princeton University Press, 1964.

16. Saltykov, Stereometric Metallography, Second Ed., Metallurgizdat, Moscow, 1958.

17. E. Underwood, Quantitative Stereology, Addison-Wesley, 1970.

18. H. Tada, P. Paris,s G. Irwin, The Stress Analysis of Cracks Handbook, Del Research Company, 1972.

19. D. Kuhlmann-Wilsdorf, Work Hardening in Tension and Fatigue, A. Thompson ed., AIME, 1975.

20. J. Foulds and J. Moteff, WRC Bulletin 269, June, 1982.

21. J. Moteff, private communication.

22. J. Hirth and Lothe, Theory of Dislocations, McGraw-Hill, 1968.

23. Metals, Reference Book, Vol. I, C. J. Smithells, ed., Plenum Press, N.Y., 1967.

24. M. Born, J. Chem. Phys. 7,591,1939.

25. M. Born, R. Furth. Proc. Cambridge Philos. Soc., 36,454,1940.

26. R. Furth, Proc. Roy. Soc. 177A, No. 969,217,1941.

27. A. Chudnovsky, in Scientific Papers on Elasticity and Plasticity, Issue 9, Leningrad University, Kachanov L.M.-ed., 1973.

1 Report No	2 Government Accession No	3 Recipient's Catalog No
NASA CR-168154		

4 Title and Subtitle	5 Report Date
CRACK LAYER MORPHOLOGY AND TOUGHNESS CHARACTERIZATION IN STEELS	May 1983
	6 Performing Organization Code

7 Author(s)	8 Performing Organization Report No
Alexander Chudnovsky and Michael Bessendorf	None
	10 Work Unit No

9 Performing Organization Name and Address	11 Contract or Grant No
Case Western Reserve University Department of Civil Engineering Cleveland, Ohio 44106	NAG-3-223
	13 Type of Report and Period Covered
12 Sponsoring Agency Name and Address	Contractor Report
National Aeronautics and Space Administration Washington, D.C. 20546	14 Sponsoring Agency Code
	505-33-22

15 Supplementary Notes

Final report. Project Manager, Bernard Gross, Structures and Mechanical Technologies Division, NASA Lewis Research Center, Cleveland, Ohio 44135.

16 Abstract

Both the macro and micro studies of crack layer propagation are presented in this report. The crack extension resistance parameter R_1 based on the morphological study of microdefects is introduced. Experimental study of the history-dependent nature of G_c supports the representation of G_c as a product of specific enthalpy of damage (material constant) and R_1. The latter accounts for the history-dependence. The observation of nonmonotonic crack growth under monotonic changes of J as well as statistical features of the critical energy release rate (variance of G_c) indicate the validity of the proposed damage characterization.

17 Key Words (Suggested by Author(s))	18 Distribution Statement
Cracks Crack growth Toughness	Unclassified - unlimited STAR Category 39

19 Security Classif (of this report)	20 Security Classif (of this page)	21 No of pages	22 Price*
Unclassified	Unclassified	40	A03

*For sale by the National Technical Information Service, Springfield, Virginia 22161

End of Document